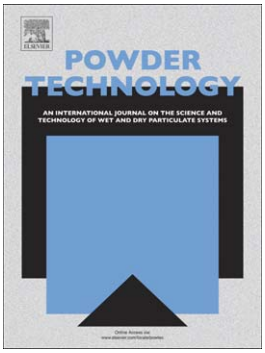

Accepted Manuscript

Effect of calcination temperature on performance of ZnO nanoparticles for dye-sensitized solar cells

Amir Moradi Golsheikh, Khosro Zangeneh Kamali, Nay Ming Huang, Ali Khorsand Zak

PII: S0032-5910(17)30944-0
DOI: doi:10.1016/j.powtec.2017.11.065
Reference: PTEC 12984

To appear in: *Powder Technology*

Received date: 23 December 2016
Revised date: 23 November 2017
Accepted date: 30 November 2017

Please cite this article as: Amir Moradi Golsheikh, Khosro Zangeneh Kamali, Nay Ming Huang, Ali Khorsand Zak, Effect of calcination temperature on performance of ZnO nanoparticles for dye-sensitized solar cells, *Powder Technology* (2017), doi:10.1016/j.powtec.2017.11.065

Effect of calcination temperature on performance of ZnO nanoparticles for dye-sensitized solar cells

Amir Moradi Golsheikh[1*], Khosro Zangeneh Kamali[2], Nay Ming Huang[3, 4], Ali Khorsand Zak[1]

[1] Nanotechnology Laboratory, Esfarayen University of Technology, 9661998195 Esfarayen, North Khorasan, Iran

[2] College of Engineering and Computer Science, Australian National University, Canberra, ACT, 2601, Australia

[3] Low Dimensional Materials Research Centre (LDMRC), Physics Department, Faculty of Science, University of Malaya, 50603 Kuala Lumpur, Malaysia

[4] Centre of Printable Electronics, Office of Deputy Vice Chancellor, University of Malaya, 50603 Kuala Lumpur, Malaysia

*Corresponding author: amir.moradi.g@gmail.com Tel: +989159006285

Abstract

The photovoltaic performances of ZnO-based dye-sensitized solar cells (DSSCs) were studied using ZnO nanoparticles prepared via the sol–gel method in gelatin medium at different calcination temperatures. The effects of the calcination temperature on the size, surface area, photoluminescence properties, and dye adsorption ability of ZnO nanoparticles were investigated. The results showed that the size of the nanoparticles increased and the surface area decreased with an increase in the calcination temperature. In addition, the oxygen vacancies of the nanoparticles increased with an increase in the calcination temperature. Moreover, although the surface area of the nanoparticles prepared at 600 °C was lower than that of those prepared at

500 °C, their dye adsorption abilities were the same, and both were higher than that of those prepared at 700 °C. Electrochemical impedance spectroscopy and open-circuit voltage decay measurements were carried out to investigate the cell functions. The DSSC based on ZnO nanoparticles calcined at 600 °C exhibited the highest conversion efficiency because of its higher dye adsorption ability and lower recombination rate compared to the others.

Keywords: ZnO; nanoparticles; gelatin; solar cell; electrochemical impedance spectroscopy; open-circuit voltage decay

1. Introduction

The study of dye-sensitized solar cells (DSSCs) has attracted attention in recent years from both the fundamental and applied points of view [1, 2]. Because of their potential low-cost and simple manufacturing, they hold promise for the mass production of photovoltaic devices [1]. In general, a typical DSSC device consists of a wide band gap semiconductor nanocrystalline porous electrode coated on a transparent conducting oxide glass (TCO), which is modified with dye (such as the ruthenium (II) complex), a counter electrode (usually Platinum), and an electrolyte solution (usually iodide-triiodide (I^-/I_3^-)) between the two electrodes [3]. Research has focused on nanostructured TiO_2 as a porous semiconductor electrode, resulting in overall conversion efficiencies exceeding 11% [2, 4, 5].

Among the semiconductor oxides that can be used as photoanode electrodes, nanostructured zinc oxide (ZnO) has emerged as a suitable alternative to TiO_2 for DSSC applications [6-9]. ZnO has a wide band gap (3.3 eV), and the energy level of its conduction band is close to that of TiO_2. However, it has a higher electron mobility and electron diffusion

coefficient. It can be easily used in a nano-architecture with a wide range of shapes and morphologies (such as nanoparticles [7, 10, 11], rods [12-14], wires [15, 16], and tubes [17]), which can be used to enhance the light absorption, dye adsorption, electron transport, and recombination properties, leading to higher conversion efficiencies. In addition to its morphology and shape, the performance of a nanostructured ZnO-based DSSC can be affected by the properties of the ZnO material, such as the type and density of the defect states [11, 18].

A variety of techniques can be used to fabricate ZnO nanostructures, including chemical bath deposition [19], sol-gel processes [20], chemical vapor deposition [21], and electrodeposition [16]. Among these techniques, sol-gel processes hold potential for the large-scale fabrication of ZnO nanomaterials. In this technique, the calcination temperature can affect the size and properties of the ZnO nanoparticles [22, 23], which can influence the performance of the ZnO in a DSSC. Studies focused on the influence of the film properties with respect to their preparation procedure and conditions such as film calcination temperature and atmosphere on the performance of both ZnO [24] and TiO_2 [25] nanostructures in a DSSC. In this study, ZnO nanoparticles were prepared using the sol-gel method in a gelatin medium as a green stabilizer at different calcination temperatures. The photo-anode electrodes were fabricated with the prepared ZnO nanoparticles at the same preparation procedure and conditions. The effects of the calcination temperature on the size of the particles, dye adsorption, charge transport and recombination, and overall conversion efficiency of DSSCs fabricated with the ZnO nanoparticles were investigated.

2. Experimental

2.1 Synthesis of ZnO nanoparticles

The ZnO nanoparticles were synthesized using a previously reported green and large-scale process, with some modification [20]. In brief, 5 g of gelatin was dissolved in 75 ml of distilled water and stirred for 30 min at 60 °C to achieve a clear gelatin solution. Then, 11 g of zinc nitrate hexahydrate was dissolved in 25 ml of distilled water and added to the gelatin solution. The temperature of the solution was fixed at 80 °C using a water bath. The solution was stirred for 8 h to obtain a brown resin. The final products were calcined at different temperatures (500, 600, and 700 °C) in air for 2 h to obtain ZnO nanoparticles.

2.2 Fabrication of DSSCs

The ZnO photo-anode electrodes were fabricated by the doctor-blade method on indium tin oxide (ITO) glass (sheet resistance: 7 Ω/sq) with the film thickness of about 15 μm. The electrodes were sintered at 150 °C for 10 min, and then annealed at 450 °C for 30 min. The annealed electrodes were soaked in an ethanolic solution of 0.3 mM N719 (Ruthenizer 535-bisTBA) dye for 90 min at room temperature under a dark condition. They were then withdrawn from the solution, washed with ethanol, and finally dried in air. A platinum-coated ITO glass was placed on a dye-sensitized photo-anode electrode, and they were clamped tightly together. An electrolyte (Iodolyte Z-100, Solaronix) solution was introduced between two electrodes using capillary action. An active area of 0.2 cm^2 was used to measure the cell performance. The current-voltage characteristics were measured using a 150 W Xenon arc lamp (Newport, Model 69907) containing a simulated AM 1.5 filter at 100 mW/cm^2. Prior to testing the photovoltaic parameter, an Avaspec-2048 fiber-optic spectrophotometer was used to measure the light illumination intensity.

3. Results and discussions

Figure 1 shows the XRD patterns of the ZnO nanoparticles prepared in the gelatin medium using different calcination temperatures. All of the peaks that appeared in the XRD patterns can be indexed to the wurtzite structure of ZnO (PDF card no: 00-005-0664). The lattice parameters were calculated and summarized in Table S1 (see supplementary information). The average crystallite sizes of the ZnO nanoparticles prepared using calcination temperatures of 500, 600, and 700 °C were 15, 18, and 22 nm, respectively, as calculated using the size strain plot method (see Figure S1). As the calcination temperature increased, the intensity of the peaks and average crystallite size increased, which indicated the formation of ZnO nanoparticles with a large average size and the enhancement of the crystallinity of the ZnO nanoparticles.

Figure 2 illustrates the representative TEM images of the ZnO nanoparticles prepared using different calcination temperatures: a) 500, b) 600, and c) 700 °C, as well as a d) high magnification HRTEM image of the ZnO nanoparticles. It can clearly be seen that the average particle size increases as the calcination temperature increases. As can be seen in the high-magnification image of the ZnO nanoparticles (Figure 2d), the measured lattice fringe space of 0.24 is attributed to the (101) plane of the ZnO, which is in agreement with the XRD results.

Figure 3 shows the room temperature photoluminescence spectra of the ZnO nanoparticles prepared at different temperatures: a) 500, b) 600, and c) 700 °C. The photoluminescence spectrum of the ZnO nanoparticles exhibits a weak ultraviolet (UV) emission peak at 386 nm and a broad visible centered peak, which is in agreement with the previous reports [26, 27]. The inset shows an enlarged image of the UV emission peak, which can be attributed to the near band edge emission. The Tauc plot of the samples showed (Figure S3), the band gap of the ZnO nanoparticles prepared at calcination temperatures of 500, 600, and 700 °C were 3.211, 3.220 and 3.223 eV, respectively, which verified the photoluminescence results. The

broad visible emission peak consists of a weak shoulder at around 453 and peaks at 542, 597, 625, and 670 nm. These may be related to the point defects, which can serve as luminescent sites. The point defects that can be presented in ZnO nanoparticles are oxygen vacancies, zinc vacancies, interstitial oxygen atoms, and interstitial zinc atoms. The weak blue emission shoulder at 453 nm may be attributed to the defect-related positively charged Zn vacancies [28]. The mechanism of the green emission (542 nm) is the most controversial. Two popular mechanisms have been proposed: 1) recombination of an electron from a level close to the conduction band edge with a deeply trapped hole in the bulk (doubly ionized oxygen vacancy (V_o^{2+})) [29] and 2) recombination of an electron in singly ionized oxygen vacancies (V_o^{+}) with a photo-generated hole in the valence band [30]. The yellow emission at 597 nm can be attributed to a doubly ionized oxygen vacancy (V_o^{2+}) and interstitial oxygen [18, 31]. The red-orange emissions at 625 and 670 nm are typically assigned to interstitial oxygen [18, 31-33]. As shown in Figure 3, although both ultraviolet and visible emission peaks are increased by raising the calcination temperature, the intensity ratio of the ultraviolet to visible emission peaks is slightly increased, which indicates a quality enhancement of the nanoparticles. Furthermore, the intensity of the peak related to the oxygen vacancy (542 nm) increases with an increase in the calcination temperature from 500 to 600 °C, which can be attributed to the increase in oxygen vacancy defects. The plausible reason is that with increasing the calcination temperature the kinetic energy of atoms in ZnO lattice will increase and the escape rate of oxygen atoms from ZnO lattice will be faster than rate of getting oxygen atoms to lattice [27, 34]. A further increase to 700 °C does not significantly change the intensity of the peak related to the oxygen vacancy.

To study the dye adsorbing capability, a certain amount of ZnO nanoparticles were dispersed in an ethanolic solution of N719 dye and kept under a dark condition for 2 h [18].

Figure 4 shows the absorption spectra of the N719 dye molecules and the separated dye molecules after dye absorption on the ZnO nanoparticles. In the absorption spectrum of the dye, two characteristic peaks can be observed at 380 and 521 nm, which are attributed to the metal-to-ligand charge-transfer (MLCT) bands. As can be seen, the intensity of the residual dye solution is almost the same for the samples prepared using 500 and 600 °C as the calcination temperature, and it is low compared to the sample prepared at 700 °C. This indicates that the dye adsorption abilities of the samples prepared using 500 and 600 °C were equal, and both were higher than that of the sample prepared at 700 °C. The measured Brunauer-Emmett-Teller (BET) surface areas for the ZnO nanoparticles prepared using 500, 600, and 700 °C as the calcination temperature were 26.7, 19.7 and 14.8 m^2/g, respectively (Figure S4). These results show that although the surface area for the sample prepared at 600 °C was smaller than that of the sample prepared at 500 °C, their dye adsorption abilities were the same. A plausible reason for this could be that the oxygen vacancies on the surface of the ZnO nanoparticles were increased by increasing the calcination temperature (as the PL results show). According to a previous report, more oxygen vacancies on the surface of nanoparticles (such as TiO_2) could induce more dye adsorption [35].

Figure 5 shows the photocurrent-voltage curves of the DSSCs fabricated with the ZnO nanoparticles prepared using different calcination temperatures for the photoanode. The characteristic parameters of the DSSCs are summarized in Table 1. As can be seen in Table 1, the ZnO nanoparticles prepared using 600 °C exhibited a higher photocurrent density, open circuit voltage, and efficiency compared to the others. The photocurrent density increased by increasing the calcination temperature from 500 °C to 600 °C. A further increase in the calcination temperature to 700 °C led to a decrease in both the photocurrent and open circuit

voltage. The performance of a DSSC could be affected by several factors such as the dye adsorbing capability, charge recombination, and charge transport.

Table 1. Characteristics of solar cells based on ZnO nanoparticles prepared at different calcination temperatures measured under AM1.5G filtered 100 mW/cm^2 illumination: short circuit current (J_{sc}), open circuit voltage (V_{oc}), fill factor (FF), and overall conversion efficiency (η).

The open-circuit voltage decay (OCVD) method upon switching off the light was used to investigate the recombination kinetics of the DSSCs. When the illumination on a DSSC was cut off, under the open circuit condition, the excess electrons could be removed by recombination. Figure 6a shows the voltage transient rate as a function of time under the open-circuit condition. The lifetime of the photo-injected electrons (τ_n) can be obtained from the OCVD data using the following equation:

$$\tau_n = -\frac{K_B T}{e}\left(\frac{dV_{OC}}{dt}\right)^{-1} \quad (1)$$

Where k_B is the Boltzman constant, T is the temperature, and e is the electronic charge. Figure 6b shows the logarithmic plot of the electron lifetime as a function of the voltage. As can be seen, the plot shows three distinct regimes of behavior. According to the mechanism of electron recombination suggested by Bisquert *et al.*[36], these regimes can be explained as follows. 1) At a high voltage, the recombination occurs through the conduction band and can be related to the free electrons, which leads to a constant electron lifetime. 2) As the voltage decreases, the electron lifetime increases linearly. This can be related to the trapping of electrons by the bulk trap states and the detrapping and recombination of the electrons to the conduction band. 3) At a low voltage, the plot of the electron lifetime changes from linear to a parabolic shape. This can be attributed to the recombination of electrons through surface traps to the fluctuating energy

levels in the electrolyte, which includes the Marcus inverted region. As can be seen in Figure 6b, the lifetime for the sample prepared using 600 °C is slightly higher than that of the sample prepared at 500 °C, and both are higher than that of the sample prepared at 700 °C. This indicates that the sample calcined at 700 °C has a higher recombination rate. In addition, when the calcination temperature increases, the parabolic shape of the lifetime becomes clear, which indicates either a surface trap density increase or that the distribution of the surface trap states become deeper [36].

The EIS method was used for the ZnO-based DSSCs to investigate the charge transport in the ZnO films and the recombination property at the film/electrolyte interface. Figure 7a and Figure S5 show the representative Nyquist plot of the ZnO based DSSCs measured at various applied bias voltages under light. All of the Nyquist plots are fitted with the equivalent circuit derived from the transmission line model of the DSSC. They all exhibit a characteristic semicircle at a high frequency, which can be associated with the resistance (R_{pt}) and capacitance (C_{pt}) of the charged platinum counter electrode/electrolyte interface. The semicircle at the low-middle frequency is due to the electron transfer (recombination) R_{ct} at the dye-sensitized ZnO nanoparticles/electrolyte interface, coupled with the electrode capacitance (denoted as chemical capacitance (C_{μ}). In addition, an approximately 45° straight-line segment can be observed at the intermediate frequency, which can be associated with the electron transport by diffusion.

Figure 7(b–d) shows the potential dependences of the charge transfer (R_{ct}), electron transport (R_t) resistance, and chemical capacitance (C_{μ}) related to the ZnO nanoparticle-based photoanodes. Figure 7b shows the semi-logarithmic variation of the charge transfer resistance, R_{ct}, as a function of the applied voltage. The exponential variation of R_{ct} can be fitted by the following equation:

$$R_{ct} = R_{0,ct} \exp\left[-\beta \frac{qV}{k_B T}\right] \quad (2)$$

where β is a parameter that can be attributed to the reaction order of the recombination reaction with respect to free electrons. The resulting β values for all of the ZnO-based photoanodes were almost the same, and are summarized in Table 2. As can be seen in Figure 7b, the ZnO-700 photoanode has the lowest recombination resistance. This can be attributed to the higher surface defects created on the surface of the ZnO nanoparticles using the higher calcination temperature. In spite of the lower surface defects in the case of the ZnO-500 photoanode, a higher recombination resistance was obtained for the ZnO-600 photoanode. This was because the dye adsorbing capabilities of the ZnO-500 and ZnO-600 nanoparticles were almost the same, and the ZnO-600 nanoparticles had a lower surface area compared to the ZnO-500 nanoparticles. Hence, the dye-coverage of the ZnO-600 photoanode was higher than that of the ZnO-500 photoanode. According to the previous reports, a higher dye-coverage leads to a lower recombination rate [37, 38]. Figure 7c shows the semi-logarithmic variation of the charge transfer resistance, R_t, as a function of the applied bias voltage corrected for the ohmic drop. As can be seen, the charge transfer resistance decreases with an increase in the calcination temperature, which could be due to an enhancement of the crystallinity by increasing the calcination temperature. Figure 7d shows the semi-logarithmic plot of the C_μ values *versus* the applied bias voltage corrected for the ohmic drop. The chemical capacitance of each of the ZnO nanoparticle-based photoanodes was exponentially increased by an increase in the applied bias voltage and can be fitted by the following equation [39]:

$$C_\mu = C_{0,\mu} \exp\left[\alpha \frac{qV}{k_B T}\right] \quad (3)$$

where k_B is the Boltzmann constant, T is the temperature (300 K), q is the elementary charge, V is the applied potential $qV=E_F-E_{redox}$, and α is a coefficient that accounts for the depth of the

exponential distribution of the trap states below the conduction band edge. The depth of the trap states could also be expressed as a temperature, T_0, according to $\alpha = T/T_0$. The parameter values of α and T_0 were consistent with the previous reports [8, 10], and are summarized in Table 2. The ZnO-700 photoanode yielded the highest T_0, which indicated a deeper distribution of states [8].

4. Conclusion

We investigated the influence of the calcination temperature on the performance of ZnO nanoparticles prepared by the sol-gel method in a gelatin medium for dye-sensitized solar cells. The calcination temperature influenced different parameters such as the size of the nanoparticles, surface area, surface defects, dye adsorption ability, and charge transfer/recombination rate, which played a decisive role in the DSSC performance. As the calcination temperature increased from 500 to 700 °C, the surface area of the nanoparticles decreased, and the surface defects such as oxygen vacancies increased. More oxygen vacancies on the surface of the nanoparticles induced more dye adsorption. Therefore, although the ZnO nanoparticles prepared at 600 °C had a lower surface area than those prepared at 500 °C, their dye adsorption abilities were the same, which led to a greater dye-coverage for the ZnO-600 photoanode. This higher dye-coverage of the ZnO-600 photoanode induced a lower recombination rate. In addition, the results showed that the charge transfer rate increased with an increase in the calcination temperature. These factors all contributed to the higher conversion efficiency of the ZnO-600 photoanode compared to the others.

Acknowledgement

This work was supported by a High Impact Research Grant from the Ministry of Higher Education of Malaysia. A. Moradi Golsheikh would like to thank Iran Nanotechnology Initiative Council.

References

[1] B. O'Regan, M. Gratzel, A low-cost, high-efficiency solar cell based on dye-sensitized colloidal TiO2 films, Nature, 353 (1991) 737-740.

[2] A. Hagfeldt, G. Boschloo, L. Sun, L. Kloo, H. Pettersson, Dye-Sensitized Solar Cells, Chem. Rev., 110 (2010) 6595-6663.

[3] M. Grätzel, Dye-sensitized solar cells, J. Photochem. Photobiol. C: Photochem. Rev., 4 (2003) 145-153.

[4] M. Grätzel, Solar Energy Conversion by Dye-Sensitized Photovoltaic Cells, Inorg. Chem., 44 (2005) 6841-6851.

[5] S. Mathew, A. Yella, P. Gao, R. Humphry-Baker, F.E. CurchodBasile, N. Ashari-Astani, I. Tavernelli, U. Rothlisberger, K. NazeeruddinMd, M. Grätzel, Dye-sensitized solar cells with 13% efficiency achieved through the molecular engineering of porphyrin sensitizers, Nat. Chem., 6 (2014) 242-247.

[6] Q. Zhang, C.S. Dandeneau, X. Zhou, G. Cao, ZnO Nanostructures for Dye-Sensitized Solar Cells, Adv. Mater., 21 (2009) 4087-4108.

[7] V.M. Guerin, C. Magne, T. Pauporté, T. Le Bahers, J. Rathousky, Electrodeposited Nanoporous versus Nanoparticulate ZnO Films of Similar Roughness for Dye-Sensitized Solar Cell Applications, ACS Appl. Mater. Interfaces, 2 (2010) 3677-3685.

[8] C. Magne, T. Moehl, M. Urien, M. Gratzel, T. Pauporte, Effects of ZnO film growth route and nanostructure on electron transport and recombination in dye-sensitized solar cells, J. Mater. Chem. A, 1 (2013) 2079-2088.

[9] A. Sacco, A. Lamberti, R. Gazia, S. Bianco, D. Manfredi, N. Shahzad, F. Cappelluti, S. Ma, E. Tresso, High efficiency dye-sensitized solar cells exploiting sponge-like ZnO nanostructures, Phys. Chem. Chem. Phys., 14 (2012) 16203-16208.

[10] E. Guillén, L.M. Peter, J.A. Anta, Electron Transport and Recombination in ZnO-Based Dye-Sensitized Solar Cells, J. Phys. Chem. C, 115 (2011) 22622-22632.

[11] K.K. Wong, A. Ng, X.Y. Chen, Y.H. Ng, Y.H. Leung, K.H. Ho, A.B. Djurišić, A.M.C. Ng, W.K. Chan, L. Yu, D.L. Phillips, Effect of ZnO Nanoparticle Properties on Dye-Sensitized Solar Cell Performance, ACS Appl. Mater. Interfaces, 4 (2012) 1254-1261.

[12] Y.F. Hsu, Y.Y. Xi, A.B. Djurišić, W.K. Chan, ZnO nanorods for solar cells: Hydrothermal growth versus vapor deposition, Appl. Phys. Lett., 92 (2008) 133507.

[13] Y. Xie, P. Joshi, S.B. Darling, Q. Chen, T. Zhang, D. Galipeau, Q. Qiao, Electrolyte Effects on Electron Transport and Recombination at ZnO Nanorods for Dye-Sensitized Solar Cells, J. Phys. Chem. C, 114 (2010) 17880-17888.

[14] C. He, Z. Zheng, H. Tang, L. Zhao, F. Lu, Electrochemical Impedance Spectroscopy Characterization of Electron Transport and Recombination in ZnO Nanorod Dye-Sensitized Solar Cells, J. Phys. Chem. C, 113 (2009) 10322-10325.

[15] J.-J. Wu, G.-R. Chen, H.-H. Yang, C.-H. Ku, J.-Y. Lai, Effects of dye adsorption on the electron transport properties in ZnO-nanowire dye-sensitized solar cells, Appl. Phys. Lett., 90 (2007) 213109.

[16] O. Lupan, V.M. Guérin, I.M. Tiginyanu, V.V. Ursaki, L. Chow, H. Heinrich, T. Pauporté, Well-aligned arrays of vertically oriented ZnO nanowires electrodeposited on ITO-coated glass and their integration in dye sensitized solar cells, J. Photochem. Photobiol. A: Chem., 211 (2010) 65-73.

[17] A.B.F. Martinson, M.S. Góes, F. Fabregat-Santiago, J. Bisquert, M.J. Pellin, J.T. Hupp, Electron Transport in Dye-Sensitized Solar Cells Based on ZnO Nanotubes: Evidence for Highly Efficient Charge Collection and Exceptionally Rapid Dynamics, J. Phys. Chem. A, 113 (2009) 4015-4021.

[18] P.P. Das, S.A. Agarkar, S. Mukhopadhyay, U. Manju, S.B. Ogale, P.S. Devi, Defects in Chemically Synthesized and Thermally Processed ZnO Nanorods: Implications for Active Layer Properties in Dye-Sensitized Solar Cells, Inorg. Chem., 53 (2014) 3961-3972.

[19] L. Vayssieres, K. Keis, A. Hagfeldt, S.-E. Lindquist, Three-Dimensional Array of Highly Oriented Crystalline ZnO Microtubes, Chem. Mater., 13 (2001) 4395-4398.

[20] A.K. Zak, W.H.A. Majid, M. Darroudi, R. Yousefi, Synthesis and characterization of ZnO nanoparticles prepared in gelatin media, Mater. Lett., 65 (2011) 70-73.

[21] E. Galoppini, J. Rochford, H. Chen, G. Saraf, Y. Lu, A. Hagfeldt, G. Boschloo, Fast Electron Transport in Metal Organic Vapor Deposition Grown Dye-sensitized ZnO Nanorod Solar Cells, J. Phys. Chem. B, 110 (2006) 16159-16161.

[22] Z.N. Kayani, F. Saleemi, I. Batool, Effect of calcination temperature on the properties of ZnO nanoparticles, Appl. Phys. A, 119 (2015) 713-720.

[23] M.R. Parra, F.Z. Haque, Aqueous chemical route synthesis and the effect of calcination temperature on the structural and optical properties of ZnO nanoparticles, J. Mater. Res. Technol. 3, (2014) 363–369.

[24] R. Marczak, F. Werner, R. Ahmad, V. Lobaz, D.M. Guldi, W. Peukert, Detailed Investigations of ZnO Photoelectrodes Preparation for Dye Sensitized Solar Cells, Langmuir, 27 (2011) 3920-3929.

[25] X. Sun, Q. Sun, Y. Li, L. Sui, L. Dong, Effects of calcination treatment on the morphology, crystallinity, and photoelectric properties of all-solid-state dye-sensitized solar cells assembled by TiO2 nanorod arrays, Phys. Chem. Chem. Phys., 15 (2013) 18716-18720.

[26] G.H. Mhlongo, O.M. Ntwaeaborwa, H.C. Swart, R.E. Kroon, P. Solarz, W. Ryba-Romanowski, K.T. Hillie, Luminescence Dependence of Pr3+ Activated SiO2 Nanophosphor on Pr3+ Concentration, Temperature, and ZnO Incorporation, J. Phys. Chem. C, 115 (2011) 17625-17632.

[27] Ö.A. Yildirım, C. Durucan, Synthesis of zinc oxide nanoparticles elaborated by microemulsion method, J. Alloys Compd., 506 (2010) 944-949.

[28] S. Kumar, S. Mukherjee, R. Kr. Singh, S. Chatterjee, A.K. Ghosh, Structural and optical properties of sol-gel derived nanocrystalline Fe-doped ZnO, J. Appl. Phys., 110 (2011) 103508.

[29] A. van Dijken, E.A. Meulenkamp, D. Vanmaekelbergh, A. Meijerink, The Kinetics of the Radiative and Nonradiative Processes in Nanocrystalline ZnO Particles upon Photoexcitation, J. Phys. Chem. B, 104 (2000) 1715-1723.

[30] K. Vanheusden, W.L. Warren, C.H. Seager, D.R. Tallant, J.A. Voigt, B.E. Gnade, Mechanisms behind green photoluminescence in ZnO phosphor powders, J. Appl. Phys., 79 (1996) 7983-7990.

[31] A.B. Djurišić, Y.H. Leung, K.H. Tam, L. Ding, W.K. Ge, H.Y. Chen, S. Gwo, Green, yellow, and orange defect emission from ZnO nanostructures: Influence of excitation wavelength, Appl. Phys. Lett., 88 (2006) 103107.

[32] L.E. Greene, M. Law, J. Goldberger, F. Kim, J.C. Johnson, Y. Zhang, R.J. Saykally, P. Yang, Low-Temperature Wafer-Scale Production of ZnO Nanowire Arrays, Angew. Chem. Int. Ed., 42 (2003) 3031-3034.

[33] D. Li, Y.H. Leung, A.B. Djurišić, Z.T. Liu, M.H. Xie, S.L. Shi, S.J. Xu, W.K. Chan, Different origins of visible luminescence in ZnO nanostructures fabricated by the chemical and evaporation methods, Appl. Phys. Lett., 85 (2004) 1601-1603.

[34] X.Q. Meng, D.Z. Shen, J.Y. Zhang, D.X. Zhao, Y.M. Lu, L. Dong, Z.Z. Zhang, Y.C. Liu, X.W. Fan, The structural and optical properties of ZnO nanorod arrays, Solid State Commun., 135 (2005) 179-182.

[35] S. Meng, E. Kaxiras, Electron and Hole Dynamics in Dye-Sensitized Solar Cells: Influencing Factors and Systematic Trends, Nano Lett., 10 (2010) 1238-1247.

[36] J. Bisquert, A. Zaban, M. Greenshtein, I. Mora-Seró, Determination of Rate Constants for Charge Transfer and the Distribution of Semiconductor and Electrolyte Electronic Energy Levels in Dye-Sensitized Solar Cells by Open-Circuit Photovoltage Decay Method, J. Am. Chem. Soc., 126 (2004) 13550-13559.

[37] M. Pazoki, P.W. Lohse, N. Taghavinia, A. Hagfeldt, G. Boschloo, The effect of dye coverage on the performance of dye-sensitized solar cells with a cobalt-based electrolyte, Phys. Chem. Chem. Phys., 16 (2014) 8503-8508.

[38] E.-H. Kong, Y.-J. Chang, J. Lim, B.-H. Kim, J.-H. Lee, D.-K. Kwon, T. Park, H.M. Jang, Bi-functional ion exchangers for enhanced performance of dye-sensitized solar cells, Chem. Comm., 49 (2013) 6671-6673.

[39] J. Bisquert, Chemical capacitance of nanostructured semiconductors: its origin and significance for nanocomposite solar cells, Phys. Chem. Chem. Phys., 5 (2003) 5360-5364.

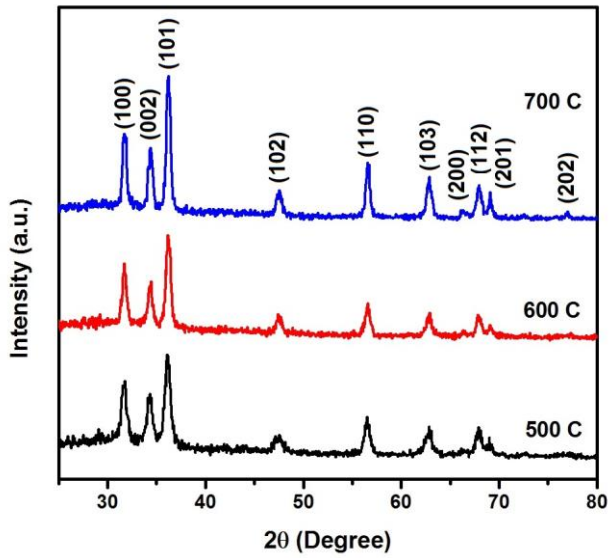

Figure 1

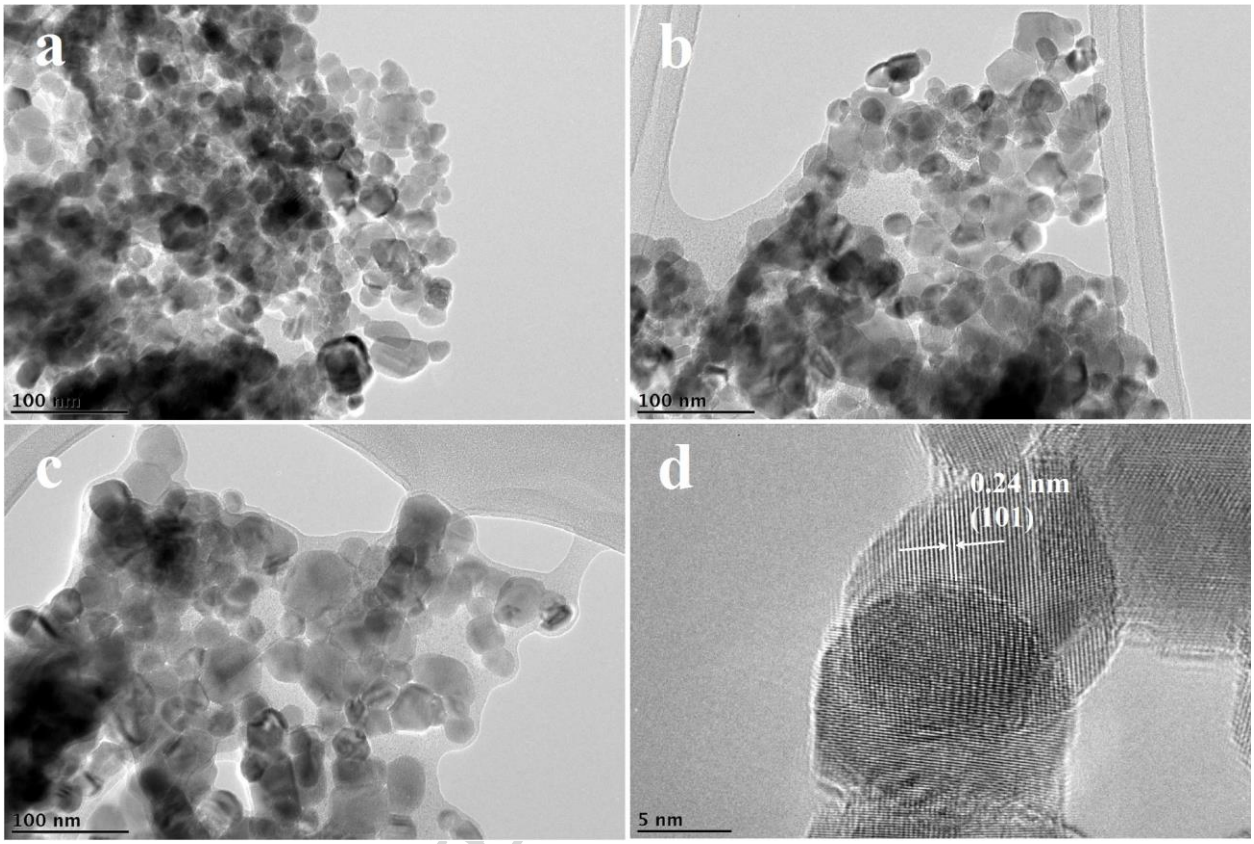

Figure 2

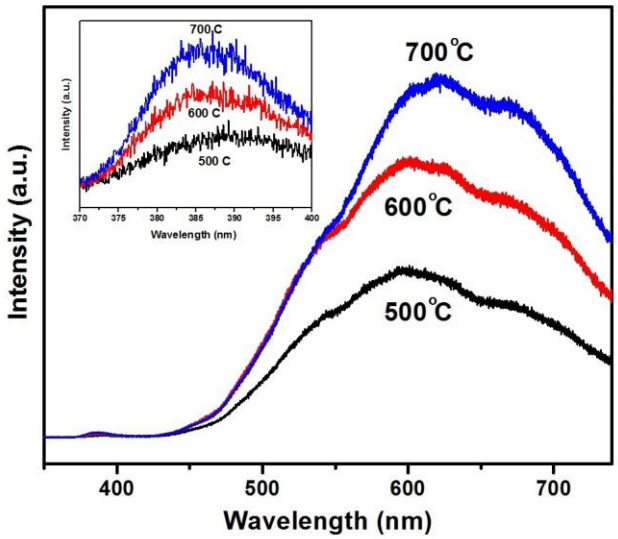

Figure 3

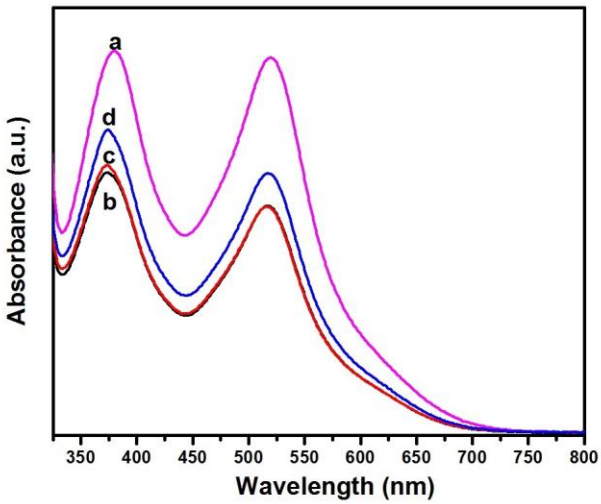

Figure 4

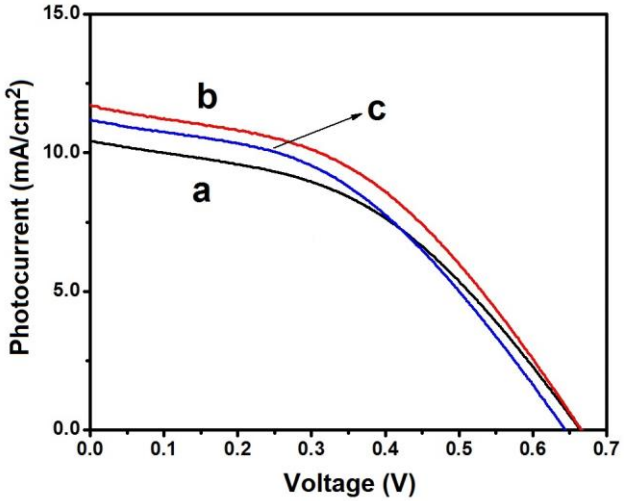

Figure 5

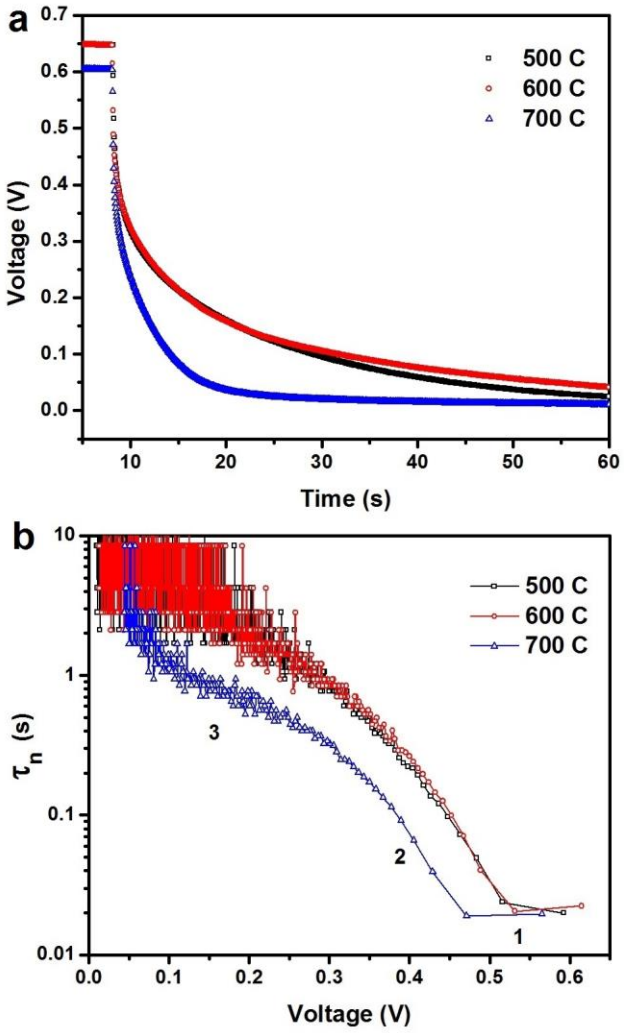

Figure 6

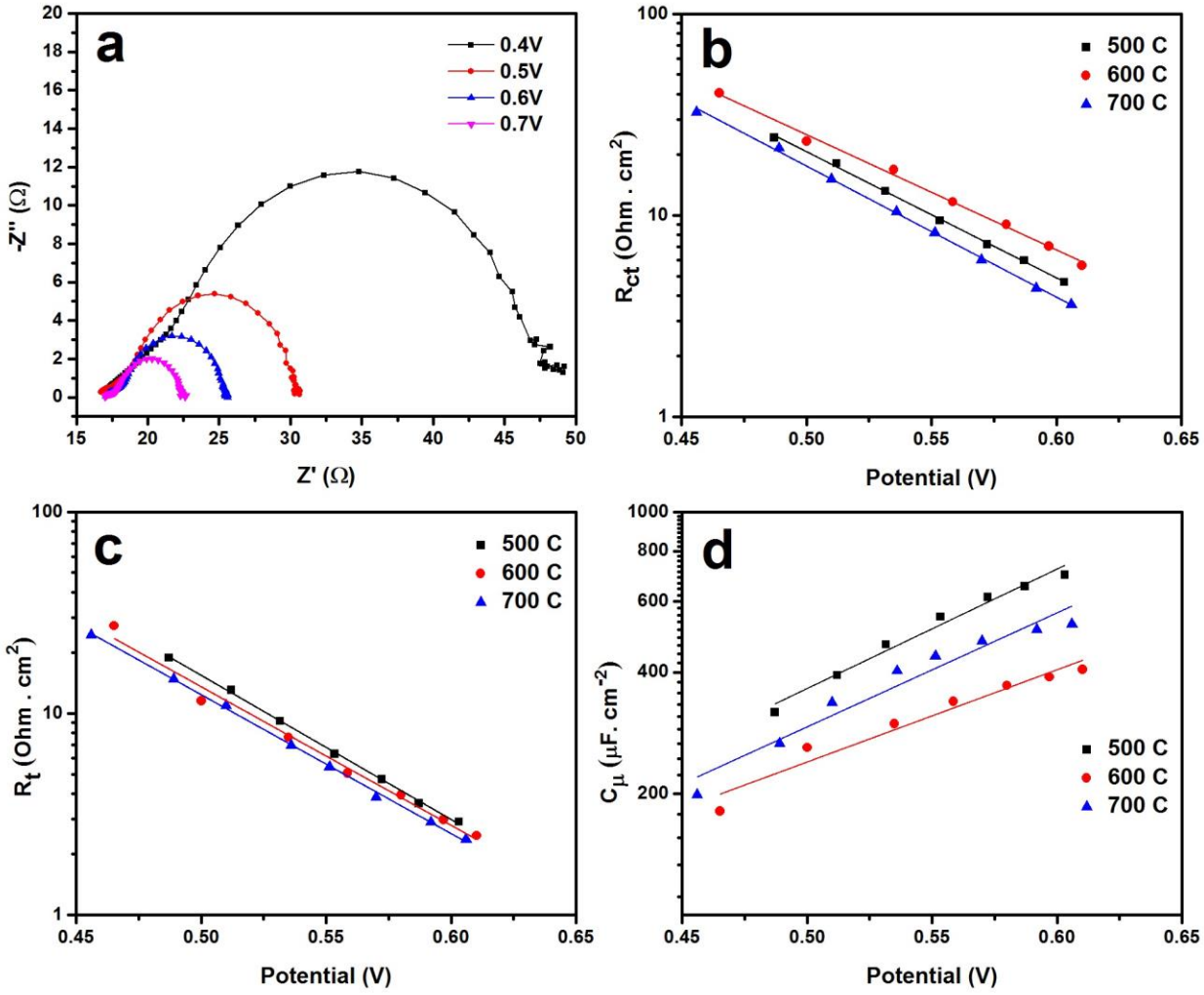

Figure 7

Table 1. Characteristics of solar cells based on ZnO nanoparticles prepared at different calcination temperatures measured under AM1.5G filtered 100 mW/cm^2 illumination: short circuit current (J_{sc}), open circuit voltage (V_{oc}), fill factor (FF), and overall conversion efficiency (η).

DSSCs	J_{sc}(mA/cm^2)	V_{oc}(mV)	FF	η(%)
ZnO-500	10.4±0.3	664±5	0.44±0.02	3.06±0.09
ZnO-600	11.7±0.2	666±6	0.44±0.01	3.44±0.1
ZnO-700	11.2±0.3	644±5	0.43±0.03	3.12±0.11

Table 2. Effects of calcination temperature on β, α, and T_0 parameters of DSSC based on ZnO nanoparticles.

DSSCs	β	α	T_0
ZnO-500	0.341	0.176	1704
ZnO-600	0.373	0.161	1863
ZnO-700	0.387	0.107	2803

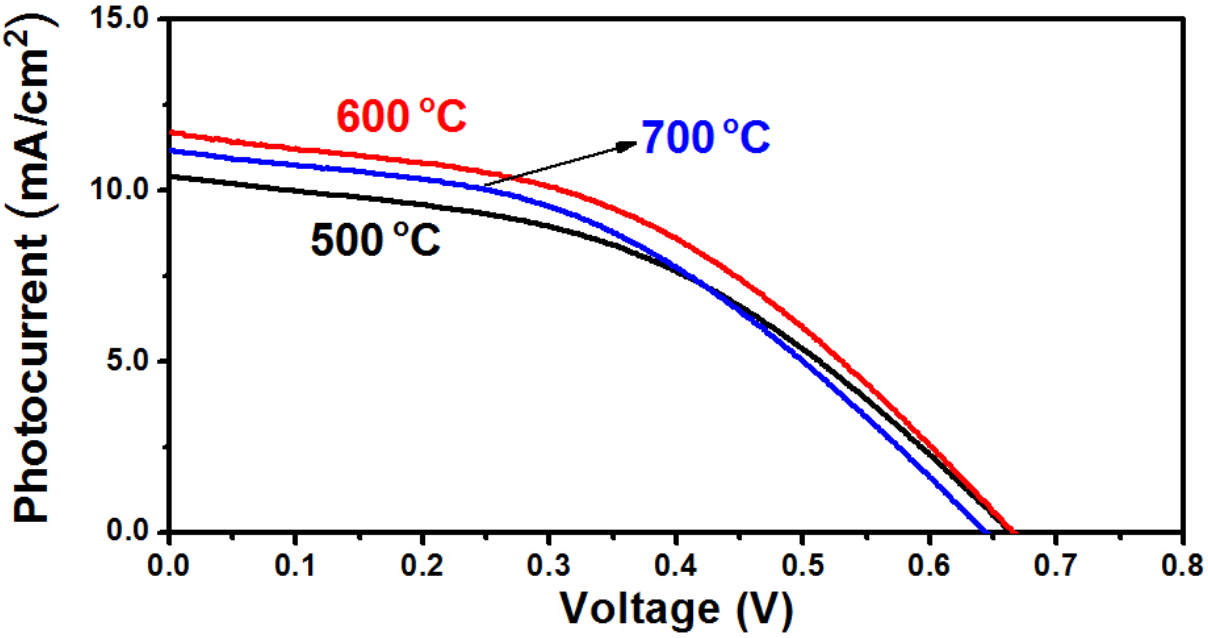

Graphical abstract

Highlights

1. ZnO nanoparticles prepared via the sol–gel method in gelatin medium at different calcination temperatures.

2. The photovoltaic performances of ZnO-based dye-sensitized solar cells were studied.

3. The calcination temperature played a decisive role in the ZnO-based DSSC performance.